Nano Energy 134 (2025) 110570

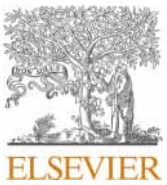

Contents lists available at ScienceDirect

Nano Energy

journal homepage: www.elsevier.com/locate/nanoen

Probing Leidenfrost effect via contact electrification☆

Roujuan Li [a,b,1], Xiang Li [a,b,1], Fujian Zhang [c], Ruishan Zhang [a], Zhongqiang Zhang [c], Zhong Lin Wang [a,*], Di Wei [a,d,**]

[a] Beijing Institute of Nanoenergy and Nanosystems, Chinese Academy of Sciences, Beijing 101400, PR China
[b] School of Nanoscience and Engineering, University of Chinese Academy of Sciences, Beijing 100049, PR China
[c] School of Mechanical Engineering, Jiangsu University, Zhenjiang 212013, PR China
[d] Centre for Photonic Devices and Sensors, University of Cambridge, 9 JJ Thomson Avenue, Cambridge CB3 0FA, UK

ARTICLE INFO

Keywords:
Contact electrification
Leidenfrost effect
Liquid-solid interface
Interface probe

ABSTRACT

Droplet dynamics and liquid-solid (L-S) interactions at elevated temperatures hold significant relevance across various industrial applications, particularly in materials design and aerospace. The Leidenfrost effect, which generates a vapor layer above a critical temperature and effectively prevents direct contact between the droplet and the heated substrate, has been extensively used in surface engineering and thermal protection. Nevertheless, the L-S interfacial properties and charge transfer at high temperatures, especially near the Leidenfrost point (LFP), have been largely neglected in past studies. This study integrated L-S contact electrification (CE) with the Leidenfrost effect, elucidating their intrinsic connection for the first time. Notably, the observation that transferred charge peaks near the LFP not only provided new theoretical insights into the temperature modulation of L-S interface properties but also presented a rapid, objective method for determining the LFP using CE as a probe. This approach holds the potential to enhance thermal management systems, improve heat dissipation in electronic devices, advance surface treatment and self-cleaning technologies, and optimize the efficiency of high-temperature self-powered equipment.

1. Introduction

The investigation of droplet behavior and liquid-solid (L-S) interfaces at elevated temperatures is vital for both everyday applications and industrial settings, ranging from materials and coatings design to aerospace engineering [1–7]. Among these phenomena, the Leidenfrost effect [8] is particularly significant. When temperatures surpass the Leidenfrost point (LFP), a continuous vapor layer forms between the solid and liquid, preventing direct contact between the droplet and the surface [9]. This phenomenon markedly reduces direct heat transfer and alters the dynamics at the solid-liquid interface [10], playing a crucial role in applications such as thermal management [11], surface protection [12,13], and self-cleaning materials [14,15]. Previous investigations into the Leidenfrost effect have primarily concentrated on vapor film formation, droplet dynamics, and heat transfer characteristics [16,17]. For instance, the vapor film formation process has been examined using high-speed photography and infrared measurements, elucidating its evolution across various materials and heating conditions [18–20]. Such studies have also clarified the instability of droplets on vapor films and its implications for heat transfer efficiency. Additionally, considerable attention has been devoted to examining the impact of diverse material and surface characteristics on the heat transfer dynamics between droplets and surfaces, analyzing factors such as surface roughness, wettability, and thermal conductivity in relation to the emergence and maintenance of the Leidenfrost effect [21,22]. While these investigations have offered valuable insights into thermal and fluid behavior, the electrical properties at high-temperature L-S interfaces have received comparatively less attention.

L-S contact electrification (CE) refers to the phenomenon of charge redistribution caused by interactions at the interface during the contact

☆ Prof Zhong Lin Wang, an author on this paper, is the Editor-in-Chief of Nano Energy, but he had no involvement in the peer review process used to assess this work submitted to Nano Energy. This paper was assessed, and the corresponding peer review managed by Professor Chenguo Hu, also an Associate Editor in Nano Energy

* Corresponding author.
** Corresponding author at: Beijing Institute of Nanoenergy and Nanosystems, Chinese Academy of Sciences, Beijing 101400, PR China.
E-mail addresses: zhong.wang@mse.gatech.edu (Z.L. Wang), dw344@cam.ac.uk (D. Wei).

[1] *These authors contributed equally to this work.*

https://doi.org/10.1016/j.nanoen.2024.110570
Received 14 November 2024; Received in revised form 3 December 2024; Accepted 9 December 2024
Available online 11 December 2024

between a solid and a liquid [23,24]. In-depth exploration of L-S CE is critical given its significant applications in energy conversion, sensing technology, and environmental monitoring, particularly amid growing demand for sustainable energy [25]. The core mechanism of L-S CE lies in charge accumulation and dissipation at the interface, i.e., charge transfer. Beyond its potential in energy harvesting and self-powered sensors, L-S CE could serve as a probe for analyzing shifts in L-S interfacial properties at room temperature. It is shown that L-S CE-based droplet triboelectric nanogenerators can obtain important information about charge transfer, charge distribution, liquid properties, and interfacial behavior, providing valuable physical and chemical insights into interfaces [26,27]. Such CE-based probe studies offer a robust tool for interface science and technology. However, at elevated temperatures, particularly near the LFP, the application of CE as a probe to examine changes in L-S interface properties remains largely unexplored.

In this study, CE as a probe was proposed to investigate the contact state and charge transfer properties of the L-S interface at high temperatures, revealing the relationship between CE and the Leidenfrost effect. Firstly, a systematic investigation was conducted on the triboelectric variations of droplets in contact with surfaces across a wide temperature range, including the LFP, with particular emphasis on droplet charging behavior near this critical point. Experimental measurements indicated that the triboelectric voltage of droplets exhibited a trend of increasing and subsequently decreasing with temperature, peaking near the LFP. This finding complemented previous limited studies of L-S CE at high temperatures and introduced a new method where CE could be employed as a probe to rapidly determine the LFP without relying on subjective judgment. Further analysis revealed that this phenomenon was attributable to variations in charge transfer between the droplet and the heated surface, linked to differences in their contact states at different temperatures. Furthermore, consistent behaviors and results were observed across salt and ethanol solutions of varying concentrations, underscoring the robustness of the conclusions and the broad applicability of the methodology. This work offered enhanced insights into the CE of droplets in high-temperature contexts, providing a theoretical foundation and practical means for designing more efficient thermal management systems and self-powered equipment. The proposed methodology of employing CE as an LFP probe is set to enable design optimization and performance enhancements across applications such as heat dissipation, electronic device cooling, aerospace material surface treatment, self-cleaning technologies, and efficiency optimization of self-powered equipment.

2. Results and discussion

Determining the state of a droplet across various temperature stages is essential for numerous applications, as droplet behavior significantly influences the efficiency and performance of specific systems [28]. As shown in Fig. 1, droplets maintained their full spherical shape at lower temperatures and were in direct contact with the surface, forming an obvious L-S interface. Due to the low surface temperature, the evaporation rate of the droplets was slower, resulting in enhanced heat transfer efficiency. This condition is particularly suitable for applications requiring gentle heat dissipation, such as cooling systems for electronic devices. As the surface temperature approached the boiling point, the droplets entered a phase of vigorous boiling. Rapid vaporization of the water at the droplet's base generated numerous bubbles, which continuously erupted from within, distorting the droplet's shape. In this phase, droplets evaporated rapidly, removing significant amounts of heat, making it ideal for use in high-efficiency heat exchange systems such as boilers and cooling towers. At the LFP, a thin vapor film was formed between the droplet and the surface, suspending the droplet without direct solid contact. The droplet stabilized into a spherical shape with a high contact angle, promoting enhanced mobility and rolling. This suspended state dramatically reduced heat transfer, causing the droplet to evaporate slowly. This phase is particularly advantageous for anti-icing and self-cleaning applications, as it reduces susceptibility to liquid contamination or freezing on surfaces.

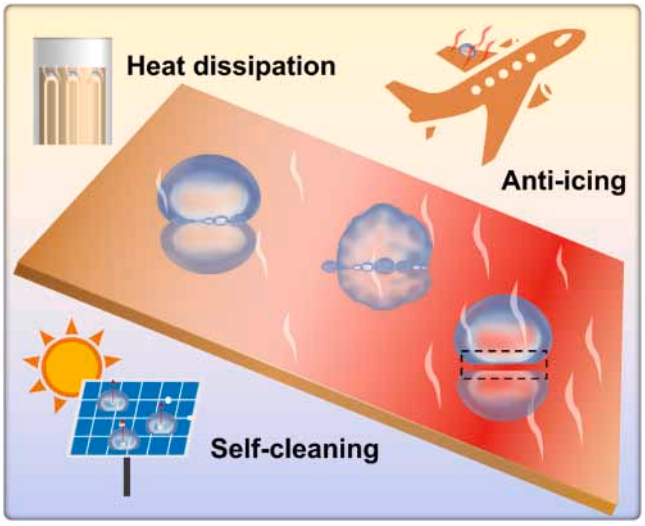

Fig. 1. Droplet states at different surface temperatures for specific applications.

2.1. Effects of temperature on the CE at L-S interfaces

To exploit the various droplet states more accurately, triboelectric signal measurements were employed to investigate the correlation between CE and the Leidenfrost effect. The experimental setup was shown in Fig. 2a. A syringe pump, grounded via the syringe, consistently dispensed approximately 20 μL droplets onto the heated surface. Three solid materials of the same size (SiO_2, Al_2O_3, Al_2O_3*) were fixed on the heating table, where Al_2O_3* represented hydrophobically treated Al_2O_3, as described in the Experimental sections. The heating table was stabilized at a controlled tilt angle of 20° to promote droplet slippage into the Faraday cylinder. The triboelectric voltage signal of the droplet as it traversed the surface of the solid material and entered the Faraday cylinder was recorded. According to the measuring principle of the electrostatic meter, the charge on the droplet is directly proportional to the measured triboelectric voltage, and the following equation relates the two :

$$V = \frac{Q}{C}$$

where Q is the charged quantity of the droplet, V is the triboelectric voltage measured by the Faraday cylinder, and C is the capacitance between the droplet and the Faraday cylinder. Under specific experimental conditions, (the structure of the Faraday cylinder, the droplet size and position are relatively stable), the triboelectric voltage could effectively reflect the amount of charge carried by the droplet. Before measuring the triboelectric signals, the LFPs for the three materials were determined to be approximately 250 °C, 200 °C, and 180 °C, respectively, as reported in the literature and confirmed through high-speed video camera analysis. To thoroughly explore the correlation between temperature and L-S CE, temperature intervals of 50 °C were selected, and the triboelectric voltage signals were measured across a broad temperature range. As depicted in Fig. 2b, the triboelectric voltage was merely 12 mV at 50 °C for the SiO_2 substrate. The triboelectric voltage gradually increased with rising temperature, peaking at approximately 18 mV near 250 °C. Subsequently, when the temperature of the heated table was further increased, the triboelectric voltage decreased considerably. A similar trend of triboelectric voltage, initially increasing and then decreasing with temperature, was also observed on the untreated Al_2O_3 ceramic sheet substrate (Fig. 2c). The maximum triboelectric voltage reached a value of approximately 145 mV at 200 °C. As the

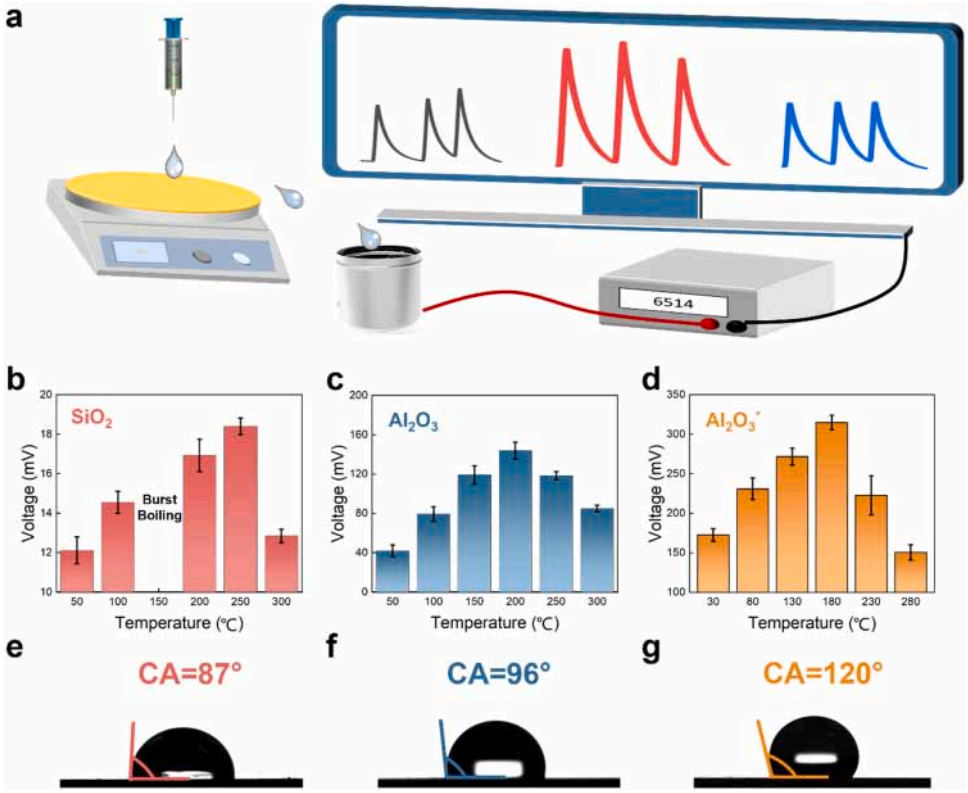

Fig. 2. Effects of temperature on the CE at L-S interfaces. (a) Experimental setup diagram for measuring the triboelectric charge of the droplets at different surface temperatures; (b) Triboelectric voltage signals of droplets measured after sliding off the SiO_2 surface at different temperatures; (c) Triboelectric voltage signals of droplets measured after sliding off the Al_2O_3 surface at different temperatures; (d) Triboelectric voltage signals of droplets measured after sliding off the Al_2O_3* surface at different temperatures; (e) The CA of static droplets on the SiO_2 surface at room temperature; (f) The CA of static droplets on the Al_2O_3 surface at room temperature; (g) The CA of static droplets on the Al_2O_3* surface at room temperature.

temperature continued to increase, the triboelectric voltage decreased steadily. It was unexpectedly found that the maximum CE occurred around the LFP, indicating that CE could be employed as a probe to rapidly determine the LFP. Furthermore, this method has been demonstrated across several materials, confirming its generalizability.

It is noteworthy that at 150 °C on SiO_2, droplets evaporated and broke up rapidly, preventing stable slip behavior and complicating the measurement of triboelectric charge. This phenomenon can be attributed to transition or burst boiling [29]. As the temperature neared but did not reach the LFP, direct contact between the droplet and substrate resulted in intense localized heating. As the temperature increased to about 200 °C, close to but not reaching the LFP, the droplets started to form a thin vapor film, reducing the direct contact with the substrate. Evaporation became relatively smooth, thus allowing slip and measurement. In contrast, such a phenomenon was not observed at 150 °C for the Al_2O_3 ceramic sheet substrate. This may be attributed to the different surface properties or the lower LFP (200 °C), which avoided the strong phase transition behavior, thereby facilitating smooth measurements across the entire temperature gradient [30,31]. On the one hand, experimental results showed that the overall CE performance of Al_2O_3 ceramic substrates was superior to that of SiO_2. Previous studies suggested that this difference could be attributed to variations in electronegativity between the materials, which is influenced by the contact area [32]. On the other hand, treatment of the Al_2O_3 surface with a small amount of perfluorosilane induced hydrophobicity, leading to the formation of hydrophobic Al_2O_3* . Energy dispersive spectroscopy (Fig. S1) confirmed a minimal presence of Si (~2 %) on the surface, indicating that the hydrophobic treatment did not significantly alter the L-S interface properties, i.e. the type of contact material. However, the difference in hydrophobicity between Al_2O_3 and Al_2O_3* emerged as a key factor in determining CE performance, which could be quantified through the measurement of the contact angle (CA) [33,34]. To further enhance CE performance, the Al_2O_3 ceramic substrate was chemically modified to improve its hydrophobicity. As illustrated in Fig. 2d, the maximum triboelectric voltage (315 mV) recorded after the droplets traversed the hydrophobized Al_2O_3* substrate occurred at approximately 180 °C, which is also near the LFP. Furthermore, Fig. 2e-g reveal that the CAs of the droplets on the SiO_2, Al_2O_3, and Al_2O_3* surfaces at room temperature were 87°, 96°, and 120°, respectively. This observation may provide a coherent framework for understanding the phenomena and principles observed in the experiments. The increased CA indicates a reduced contact area between the droplet and the surface, effectively diminishing the heat transfer efficiency and making the droplet less susceptible to rapid vaporization or bursting behavior. Additionally, Fig. S2 demonstrated that the variance in wettability between SiO_2 and Al_2O_3 is primarily attributable to their respective surface structures. Chemical modification enhances the Al_2O_3 surface by incorporating more hydrophobic chemical compositions.

2.2. *Mechanistic analysis of temperature-dependent variations in CE*

To investigate the mechanisms underlying variations in CE across a broad temperature spectrum, experiments were conducted on Al_2O_3* substrates at temperatures of 100 °C and 190 °C, utilizing droplets with a volume of 20 μL. Among them, 100 °C was used to probe the high-temperature CE when the LFP was not reached, while 190 °C ensured that the triboelectric signals in the state of reaching the LFP were obtained. It should be noted that Fig. 3a examined the change in triboelectric voltage with varying sliding distances while keeping sliding time short (less than 1 s) to avoid evaporation influence, whereas Fig. 3b investigated the change in triboelectric voltage with a constant sliding distance (6 cm) and varying sliding time, achieved by adjusting the tilt

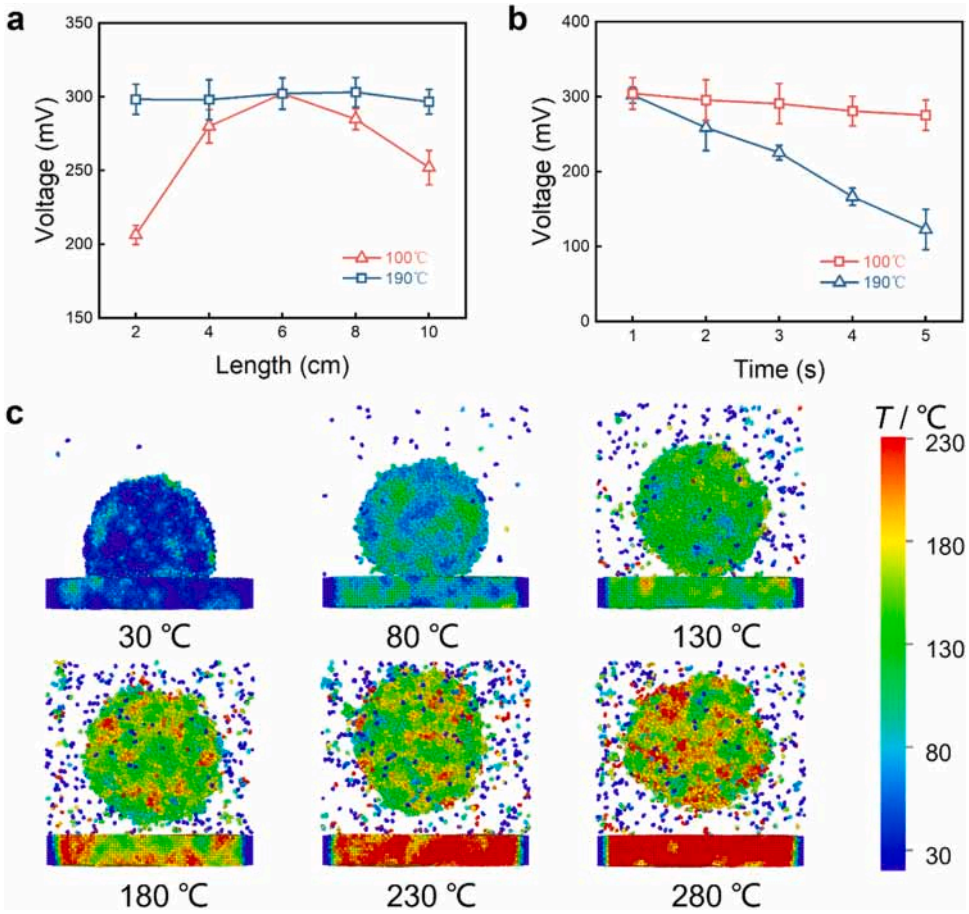

Fig. 3. Potential mechanisms of CE variation across a broad temperature spectrum. (a) Effect of the sliding length of droplets on the Al_2O_3* surface at different temperatures on the measured triboelectric voltage signal; (b) Effect of the residence time of droplets on the Al_2O_3* surface at different temperatures on the measured triboelectric voltage signal; (c) Simulation of the contact state when the temperature of droplets on the substrate surface was stable at different temperatures.

angle of the substrate. Firstly, the distance over which the droplet slides on the Al_2O_3* substrate gradually grew from 2 to 10 cm, ensuring that the droplet release height and other conditions were the same. As shown in Fig. 3a, the sliding distance of the droplet on the heated surface was first varied. At 100 °C, the triboelectric voltage signal initially increased and then decreased with increasing distance, reaching a maximum at a sliding distance of 6 cm. At this temperature, the droplet remained in direct contact with the substrate. Initially, there was less charge transfer due to lower temperature. The increase in sliding distance enhanced the L-S CE, leading to a rise in the triboelectric voltage. However, as the sliding distance became too long, the retention of the droplet on the surface resulted in the charge within the droplet being partially residual on the surface, and the triboelectric voltage then decreased. In contrast, as the temperature increased to 190 °C, the droplets were in the Leidenfrost effect state, where they were suspended above the vapor film. In this case, the charge residue of the droplets on the surface was minimal. It was worth mentioning that the droplets moved on the surface for a short time (less than 1 s) in Fig. 3a, so the effect of evaporation was small. Furthermore, as shown in Fig. 3b, the retention time of the droplets on the surface increased progressively, while the sliding distance was maintained at the optimized value of 6 cm, as depicted in Fig. 3a. The experimental results showed that the triboelectric voltage of the droplets at 100 °C decreased slightly as the residence time on the surface increased. In contrast, at 190 °C, the evaporation process accelerated, leading to a rapid decrease in the triboelectric voltage. In summary, under short sliding time (less than 1 s), the decrease in triboelectric voltage was attributed to the retention of charge within the droplet, which partially remained on the surface. However, as the sliding time and/or temperature increased, the evaporation of the droplets was promoted, leading to a further reduction in triboelectric voltage. As illustrated in Fig. S3, this phenomenon was observed not only in Al_2O_3* but also in experiments conducted on SiO_2 substrates at 100 °C and 260 °C, ensuring the Leidenfrost state. These observations underscore the intricate interplay of contact, charge transfer, and thermodynamic behavior at the L-S interface, particularly at elevated temperatures where droplet behavior is influenced by the Leidenfrost effect. To further demonstrate that the differences in CE were caused by the different contact states of the droplets with the surface, simulations were performed using the open-source software LAMMPS. The specific parameters were shown in the Supplementary discussion. The substrate temperature was set to 30 ℃, 80 ℃, 130 ℃, 180 ℃, 230 ℃, and 280 ℃, respectively. The temperature contour map of the droplet on substrates at different temperatures is shown in Fig. 3c. As the substrate temperature increases from 30 ℃ to 80 ℃, the contact angle of the droplet decreases, as higher temperatures reduce the surface tension of the droplet. Then, when the substrate temperature increases to 130 ℃, the contact area between the droplet and substrate decreases because the rapid evaporation of water molecules at the liquid-solid interface lifts the droplet. Finally, as the substrate temperature continues to rise, the droplet gradually detaches from the substrate at 180 ℃, and a distinct levitation state is observed at 230 ℃ and 280 ℃.

2.3. Probing LFP via CE

As an important factor influencing the LFP, droplet volume was explored. 10 μL of deionized water on an Al_2O_3* substrate was

performed with a temperature gradient of 10 °C. As shown in Fig. S4, the maximum value of the triboelectric voltage occurred near 170 °C, reaching approximately 238 mV. This observation was consistent with the LFP identified in both the literature and high-speed camera measurements [35]. To establish the reliability and generalizability of that CE could be employed as a probe to rapidly determine LFP, a range of solutions was experimentally evaluated in place of deionized water. Specifically, NaCl solution (characterized by the minimal size difference between cations and anions) and room-temperature ionic liquid [EMIM]Cl (with asymmetric cation-anion pairs) were first chosen to explore the behavior of droplets from different ionic types of solutions. The hydrophobic Al_2O_3* substrate material was placed on a heated bench and experiments were carried out with a temperature gradient of 50 °C. 20 μL droplets were slid from the substrate into a Faraday cylinder to measure the triboelectric charge. A discernible trend of the triboelectric voltage initially increasing and subsequently decreasing with rising temperature was consistently observed. As shown in Fig. 4a, the maximum value of the triboelectric signal was observed near 180 °C for a 0.001 M NaCl droplet. To present the experimental results more clearly, the temperature gradient was reduced to 5 °C, and the triboelectric signals within 180 °C-200 °C were specifically viewed. The maximum value of the triboelectric voltage measured for a 0.001 M NaCl droplet was about 403 mV, which was closer to 185 °C. Increasing the NaCl concentration to 0.1 M, the maximum friction electric voltage under the same conditions occurs at 190 °C (284 mV). The decrease in transferred charge may be due to the shielding effect of the electrical double layer [36]. Excitingly, the observation that the peak triboelectric voltage in solution shifts to higher temperatures with increasing solubility aligns perfectly with the literature on the LFP [37], further substantiating the reliability of determining the LFP through CE. This phenomenon could be attributed to the influence of precipitated salts. At lower concentrations, there is less salt precipitation, resulting in minimal alterations to the properties of the droplets. At higher concentrations of NaCl solutions, solid salt precipitated at high temperatures might form a barrier layer between the droplet and the substrate, affecting the formation of the vapor film and ultimately increasing the LFP. As illustrated in Fig. S5, the precipitation of salt was observable on the surface following the complete evaporation of the droplets. A similar pattern was noted in [EMIM]Cl (Fig. 4a and b). In contrast, the presence of asymmetric ions at high concentrations induced a reversal of the polarity of the triboelectric voltage at lower temperatures [38]. Nevertheless, this alteration did not compromise that CE could be employed as a probe to rapidly determine LFP, further underscoring the method's generalizability.

In addition to saline solutions, CE as a probe for rapid determination of LFP was applied in organic solvents. 20 μL of 5 % ethanol (v/v) and 10 % ethanol (v/v) were chosen respectively, where "v/v" stands for volume/volume ratio. The measured triboelectric voltage increased and then decreased as the temperature increased. For 5 % ethanol, the highest value of the triboelectric voltage was found to occur at 175 °C after narrowing the temperature gradient, which was about 220 mV (Fig. 5a). The highest value of the triboelectric voltage for 10 % ethanol decreased to 170 °C, which was about 199 mV (Fig. 5b). The decrease in the charge transfer might be attributed to the fact that as the

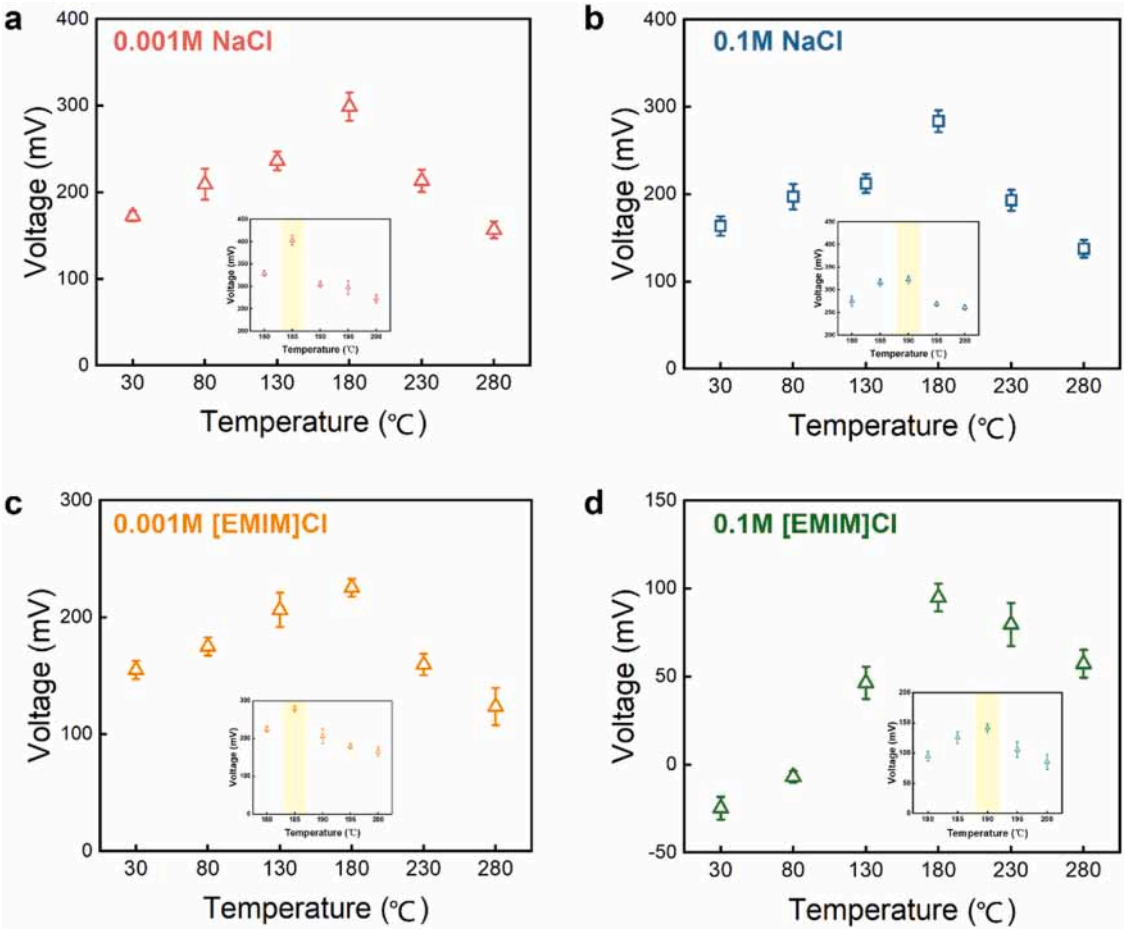

Fig. 4. Probing LFP via triboelectric charge. (a) Triboelectric voltage signals were measured after sliding the 0.001 M NaCl droplets off the surface at different temperatures; (b) Triboelectric voltage signals were measured after sliding the 0.1 M NaCl droplets off the surface at different temperatures; (c) Triboelectric voltage signals were measured after sliding the 0.001 M [EMIM]Cl droplets off the surface at different temperatures; (d) Triboelectric voltage signals were measured after sliding the 0.1 M [EMIM]Cl droplets off the surface at different temperatures.

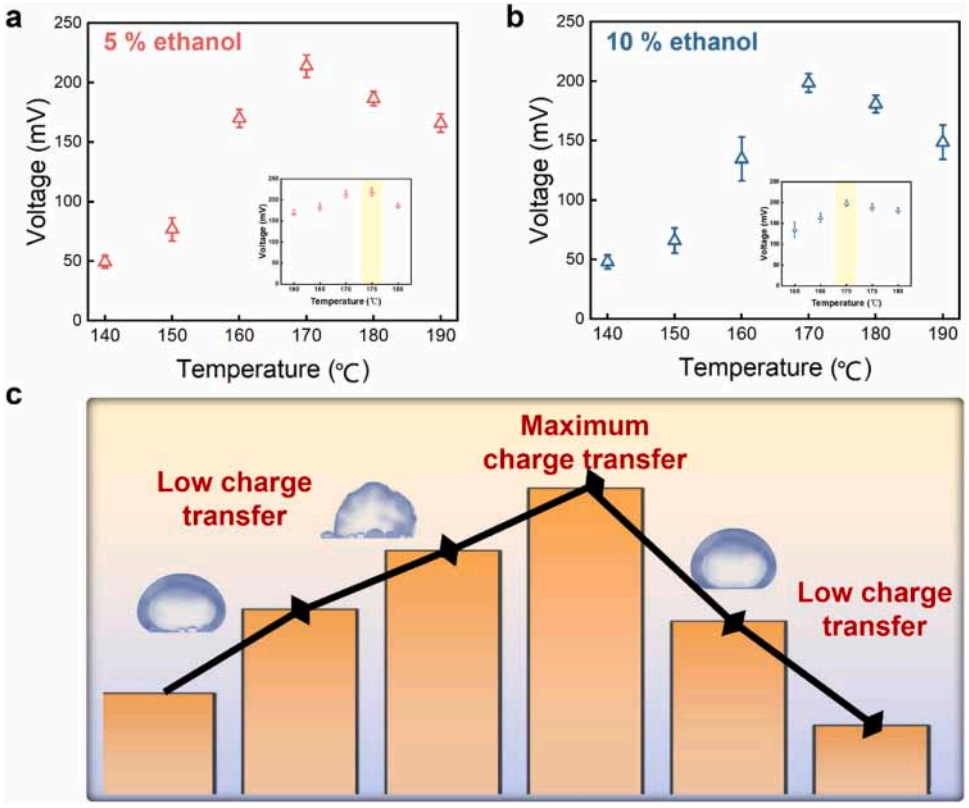

Fig. 5. Relationship and Applications of CE and LFP. (a) Triboelectric voltage signals were measured after sliding the 5 % ethanol droplets off the surface at different temperatures; (b) Triboelectric voltage signals were measured after sliding the 10 % ethanol droplets off the surface at different temperatures; (c) Relationship between CE with Leidenfrost effect and application to high-temperature self-powered equipment.

concentration of ethanol increased, the rate of evaporation of the solution became faster [39]. It made the contact time of the droplets on the surface shorter, thus affecting the strength of the CE. In the near vicinity of the LFP, the droplets were suspended on the solid surface due to surface tension and the formation of a surface vapor film. An increase in ethanol concentration will change the contact angle and surface tension of the droplets. 10 % ethanol droplets might form a complete vapor film earlier than 5 % ethanol droplets and therefore had a lower LFP. It is satisfying to observe that the trends of the two still align remarkably well [40].

By investigating the relationship between CE and the Leidenfrost effect, an interesting and universal pattern was found: with increasing temperature, the transferred charge of a droplet sliding on a surface did not change linearly, but showed a tendency to increase and then decrease. This phenomenon offered us a new way to quickly and objectively discriminate LFP by measuring changes in droplet triboelectric voltage or transferred charge, avoiding the subjectivity and complexity of traditional methods that rely on visual observation and indirect measurements by heat transfer. This means of rapid discrimination of LFP was not only of great value in academic research but can also be useful in many practical applications. Especially in some experiments and industrial processes related to surface engineering, material treatment, and surface effects that need to be performed at high temperatures, such as heat dissipation, anti-icing, and self-cleaning. More importantly, based on this phenomenon, it could be further applied to high-temperature self-powered equipment. Nowadays, CE has been widely used in many fields, such as electrostatic sensors, electrostatic dust removal, and energy harvesting [41]. However, how to improve the efficiency and the amount of charge transferred by CE in a high-temperature environment has always been an urgent challenge. By applying the results of the study of the relationship between CE and LFP to these devices, it will be possible to maximize the amount of charge transferred by the self-powered equipment at high temperatures, thereby enhancing their operating efficiency (Fig. 5c). Specifically, in design of the device, the temperature of the surface will be controlled to stabilize the operating temperature in the interval close to the LFP. Within this temperature range, the amount of charge transferred by the device will peak, ensuring the most efficient charge transfer. This is particularly important for energy harvesting devices, as an increase in transferred charge directly implies an increase in the output power of the device. Additionally, in industrial processes where stable charge transfer and efficient electrostatic effects are required, such as electrostatic separation, dust handling, and spraying processes, this finding could also greatly improve the stability and efficiency of the self-powered equipment.

3. Conclusion

This work revealed the charged properties of droplets at elevated L-S temperatures and explored the intrinsic relationship between CE and the Leidenfrost effect, proposing CE as an efficient probe for LFP determination. Systematic experimental studies show that the triboelectric voltage of droplets initially increases, peaks near the LFP, and then decreases with rising temperature. These findings provide new theoretical insights into the temperature-driven modulation of L-S interface properties. Moreover, a rapid and objective method for LFP determination using CE has been introduced for a wide range of solid and liquid materials. This approach fills a critical gap in interfacial probes for high-temperature L-S CE studies, introducing a new and universally applicable technique for LFP analysis. The CE-based probe technique offers advantages over traditional methods (e.g., optical or surface potential analysis), such as high sensitivity, no need for complex equipment, and weak subjective dependence. The results may be affected by the experimental environment (e.g., humidity), and the maturity of the

technique will be further improved in the future. This work enhances the understanding of CE in elevated temperatures, providing theoretical support for the design of thermal management systems, novel sensors, and related technologies. It is set to propel efficiency optimization in high-temperature self-powered devices, catalyzing advancements in heat dissipation, aerospace materials, and self-cleaning technologies.

4. Experimental section

4.1. Chemicals and materials

Sodium chloride (NaCl) (≥99 %) and 1-Ethyl-3-methylimidazolium Chloride([EMIM]Cl) (98 %) was purchased from Aladdin. 1 H,1 H,2 H,2H-Perfluorodecyltriethoxysilane (PFDS) was from Macklin. The silicon dioxide (SiO_2), aluminum oxide (Al_2O_3) ceramic sheet, ethanol and laboratory-prepared deionized water were purchased from the local market. Syringes were purchased from local pharmacies.

4.2. Fabrication of Al_2O_3*

Firstly, the Al_2O_3 ceramic sheet was cleaned using anhydrous ethanol in an ultrasonic cleaner for 15 minutes to remove surface dirt and organic contaminants. After that, the Al_2O_3 was rinsed with deionized water followed by rinsing with anhydrous ethanol, and subsequently placed in a drying oven at 60 °C for half an hour. Next, the 1 % PFDS solution was prepared by dilution with anhydrous ethanol. The dried ceramic sheet was immersed in the prepared 1 % PFDS solution, ensuring that it was completely submerged, at room temperature for 3 h. After removal, the surface was gently rinsed with anhydrous ethanol to remove excess PFDS solution. Finally, the treated ceramic sheets were placed in a drying oven at 150°C for 1 h to promote the chemical bonding of PFDS to the surface. After curing, the Al_2O_3* were removed and cooled to room temperature.

4.3. Electrical and optical characterization

The charge of the droplets was tested using an electrometer (6514, Keithley, Cleveland, OH, USA) and a Faraday cylinder. Real-time data collection was achieved using a platform built on a data acquisition card (BNC-2120, National Instruments, Austin, TX, USA) and LabView software. The topographical features of the samples were observed using a scanning electron microscope and the surface chemical composition was analyzed by EDS. Water's static contact angles were determined using a DSA-100 optical CA meter (Kruss Company, Ltd., Germany) with a test temperature set at room temperature.

CRediT authorship contribution statement

Di Wei: Writing – review & editing, Supervision, Resources, Project administration, Methodology, Funding acquisition, Formal analysis, Conceptualization. **Zhong Lin Wang:** Resources, Project administration, Formal analysis. **Fujian Zhang:** Visualization, Software. **Xiang Li:** Writing – review & editing, Project administration, Methodology, Formal analysis, Conceptualization. **Zhongqiang Zhang:** Software, Resources. **Ruishan Zhang:** Validation, Investigation. **Roujuan Li:** Writing – original draft, Visualization, Validation, Investigation, Formal analysis, Data curation, Conceptualization.

Declaration of Competing Interest

The authors declare no competing interests.

Acknowledgments

The authors are grateful for the support received from the National Natural Science Foundation (Grant No. 22479016) and appreciate the technical assistance from the instrument & equipment platform of the Beijing Institute of Nanoenergy and Nanosystems.

Appendix A. Supporting information

Supplementary data associated with this article can be found in the online version at doi:10.1016/j.nanoen.2024.110570.

Data availability

No data was used for the research described in the article.

References

[1] X. Yu, Y. Zhang, R. Hu, X. Luo, Water droplet bouncing dynamics, Nano Energy 81 (2021) 105647, https://doi.org/10.1016/j.nanoen.2020.105647.
[2] J. Li, Y. Hou, Y. Liu, C. Hao, M. Li, M.K. Chaudhury, S. Yao, Z. Wang, Directional transport of high-temperature Janus droplets mediated by structural topography, Nat. Phys. 12 (2016) 606–612, https://doi.org/10.1038/nphys3643.
[3] H.J. Cho, D.J. Preston, Y. Zhu, E.N. Wang, Nanoengineered materials for liquid–vapour phase-change heat transfer, Nat. Rev. Mater. 2 (2016) 16092, https://doi.org/10.1038/natrevmats.2016.92.
[4] K.N. Nampoothiri, M.S. Seshasayee, V. Srinivasan, M.S. Bobji, P. Sen, Direct heating of aqueous droplets using high frequency voltage signals on an EWOD platform, Sens. Actuators B Chem. 273 (2018) 862–872, https://doi.org/10.1016/j.snb.2018.06.091.
[5] C. Liu, C. Lu, Z. Yuan, C. Lv, Y. Liu, Steerable drops on heated concentric microgroove arrays, Nat. Commun. 13 (2022) 3141, https://doi.org/10.1038/s41467-022-30837-z.
[6] J. Yang, Y. Li, D. Wang, Y. Fan, Y. Ma, F. Yu, J. Guo, L. Chen, Z. Wang, X. Deng, A standing Leidenfrost drop with Sufi whirling, Proc. Natl. Acad. Sci. U. S. A. 120 (2023) e2305567120, https://doi.org/10.1073/pnas.2305567120.
[7] M. Jiang, Y. Wang, F. Liu, H. Du, Y. Li, H. Zhang, S. To, S. Wang, C. Pan, J. Yu, D. Quéré, Z. Wang, Inhibiting the Leidenfrost effect above 1,000 °C for sustained thermal cooling, Nature 601 (2022) 568–572, https://doi.org/10.1038/s41586-021-04307-3.
[8] A.-L. Biance, C. Clanet, D. Quéré, Leidenfrost drops, Phys. Fluids 15 (2003) 1632–1637, https://doi.org/10.1063/1.1572161.
[9] A. Bouillant, T. Mouterde, P. Bourrianne, A. Lagarde, C. Clanet, D. Quéré, Leidenfrost wheels, Nat. Phys. 14 (2018) 1188–1192, https://doi.org/10.1038/s41567-018-0275-9.
[10] D. Quéré, Leiden.-. Dyn. 45 (2013) 197–215, https://doi.org/10.1146/annurev-fluid-011212-140709.
[11] D. Saranadhi, D. Chen, J.A. Kleingartner, S. Srinivasan, R.E. Cohen, G.H. McKinley, Sustained drag reduction in a turbulent flow using a low-temperature Leidenfrost surface, Sci.Adv. 2 e1600686. https://doi.org/10.1126/sciadv.1600686.
[12] S.M. Sajadi, P. Irajizad, V. Kashyap, N. Farokhnia, H. Ghasemi, Surfaces for high heat dissipation with no Leidenfrost limit, Appl. Phys. Lett. 111 (2017) 021605, https://doi.org/10.1063/1.4993775.
[13] R. van Erp, R. Soleimanzadeh, L. Nela, G. Kampitsis, E. Matioli, Co-designing electronics with microfluidics for more sustainable cooling, Nature 585 (2020) 211–216, https://doi.org/10.1038/s41586-020-2666-1.
[14] S. Lyu, V. Mathai, Y. Wang, B. Sobac, P. Colinet, D. Lohse, C. Sun, Final fate of a Leidenfrost droplet: Explosion or takeoff, Sci.Adv. 5 eaav8081. https://doi.org/10.1126/sciadv.aav8081.
[15] S.R. Waitukaitis, A. Zuiderwijk, A. Souslov, C. Coulais, M. van Hecke, Coupling the Leidenfrost effect and elastic deformations to power sustained bouncing, Nat. Phys. 13 (2017) 1095–1099, https://doi.org/10.1038/nphys4194.
[16] J.C. Burton, A.L. Sharpe, R.C.A. van der Veen, A. Franco, S.R. Nagel, Geometry of the vapor layer under a Leidenfrost drop, Phys. Rev. Lett. 109 (2012) 074301, https://doi.org/10.1103/PhysRevLett.109.074301.
[17] J. Kistemaker, The spheroidal state of a waterdrop: The leidenfrost phenomenon, Physica 29 (1963) 96–104, https://doi.org/10.1016/S0031-8914(63)80194-9.
[18] A. Shahriari, J. Wurz, V. Bahadur, Heat transfer enhancement accompanying Leidenfrost state suppression at ultrahigh temperatures, Langmuir 30 (2014) 12074–12081, https://doi.org/10.1021/la502456d.
[19] A. Shahriari, S. Das, V. Bahadur, R.T. Bonnecaze, Analysis of the instability underlying electrostatic suppression of the Leidenfrost state, Phys. Rev. Fluids 2 (2017) 034001, https://doi.org/10.1103/PhysRevFluids.2.034001.
[20] O. Ozkan, A. Shahriari, V.J.A.P.L. Bahadur, Electrostatic suppression of the Leidenfrost state using AC electric fields 111 (2017) 141608, https://doi.org/10.1063/1.4999174.
[21] V. Talari, P. Behar, Y. Lu, E. Haryadi, D. Liu, Leidenfrost drops on micro/nanostructured surfaces, Front. Energy 12 (2018) 22–42, https://doi.org/10.1007/s11708-018-0541-7.
[22] H. Kim, B. Truong, J. Buongiorno, L.-W. Hu, On the effect of surface roughness height, wettability, and nanoporosity on Leidenfrost phenomena, Appl. Phys. Lett. 98 (2011) 083121, https://doi.org/10.1063/1.3560060.
[23] M. Sun, Q. Lu, Z.L. Wang, B. Huang, Understanding contact electrification at liquid–solid interfaces from surface electronic structure, Nat. Commun. 12 (2021) 1752, https://doi.org/10.1038/s41467-021-22005-6.

[24] Y. Jin, S. Yang, M. Sun, S. Gao, Y. Cheng, C. Wu, Z. Xu, Y. Guo, W. Xu, X. Gao, S. Wang, B. Huang, Z. Wang, How liquids charge the superhydrophobic surfaces, Nat. Commun. 15 (2024) 4762, https://doi.org/10.1038/s41467-024-49088-1.
[25] X. Li, Z.L. Wang, D. Wei, Scavenging energy and information through dynamically regulating the electrical double layer, Adv. Funct. Mater. 34 (2024) 2405520, https://doi.org/10.1002/adfm.202405520.
[26] J. Zhang, S. Lin, Z.L. Wang, Triboelectric nanogenerator array as a probe for in situ dynamic mapping of interface charge transfer at a liquid–solid contacting, ACS Nano 17 (2023) 1646–1652, https://doi.org/10.1021/acsnano.2c11633.
[27] J. Zhang, S. Lin, M. Zheng, Z.L. Wang, Triboelectric nanogenerator as a probe for measuring the charge transfer between liquid and solid surfaces, ACS Nano 15 (2021) 14830–14837, https://doi.org/10.1021/acsnano.1c04903.
[28] A. Bouillant, C. Cohen, C. Clanet, D. Quéré, Self-excitation of Leidenfrost drops and consequences on their stability, Proc. Natl. Acad. Sci. U. S. A. 118 (2021) e2021691118, https://doi.org/10.1073/pnas.2021691118.
[29] H. Jo, H.S. Ahn, S. Kang, M.H. Kim, A study of nucleate boiling heat transfer on hydrophilic, hydrophobic and heterogeneous wetting surfaces, Int. J. Heat. Mass Transf. 54 (2011) 5643–5652, https://doi.org/10.1016/j.ijheatmasstransfer.2011.06.001.
[30] S. Ogata, R. Nakanishi, Effect of surface textures and wettability on droplet impact on a heated surface, Processes 9 (2021) 350, https://doi.org/10.3390/pr9020350.
[31] L. Zhong, Z. Guo, Effect of surface topography and wettability on the Leidenfrost effect, Nanoscale 9 (2017) 6219–6236, https://doi.org/10.1039/C7NR01845B.
[32] N. Wang, Y. Liu, E. Ye, Z. Li, D. Wang, Contact electrification behaviors of solid–liquid interface: regulation, mechanisms, and applications, Adv. Energy Sustain. Res. 4 (2023) 2200186, https://doi.org/10.1002/aesr.202200186.
[33] A. Kulandaivel, S. Potu, R.K. Rajaboina, U.K. Khanapuram, Exploring wettability: a key to optimizing liquid–solid triboelectric nanogenerators, ACS Appl. Mater. Interfaces 16 (2024) 58029–58059, https://doi.org/10.1021/acsami.4c10063.
[34] X. Li, L. Zhang, Y. Feng, X. Zhang, D. Wang, F. Zhou, Solid–liquid triboelectrification control and antistatic materials design based on interface wettability control, Adv. Funct. Mater. 29 (2019) 1903587, https://doi.org/10.1002/adfm.201903587.
[35] B. Zabala, A. Igartua, V. Scarpis, G. Timelli, F. Girot, R. Nevshupa, Multiparametric study of Leidenfrost point and wettability of lubricants on high-pressure die-casting dies, Int. J. Therm. Sci. 125 (2018) 66–73, https://doi.org/10.1016/j.ijthermalsci.2017.11.014.
[36] X. Li, S. Li, X. Guo, J. Shao, Z.L. Wang, D. Wei, Triboiontronics for efficient energy and information flow, Matter 6 (2023) 3912–3926, https://doi.org/10.1016/j.matt.2023.08.022.
[37] C.-K. Huang, V.P. Carey, The effects of dissolved salt on the Leidenfrost transition, Int. J. Heat. Mass Transf. 50 (2007) 269–282, https://doi.org/10.1016/j.ijheatmasstransfer.2006.06.031.
[38] R. Li, X. Li, Z. Zhang, M. Willatzen, Z.L. Wang, D. Wei, Triboelectric programmed droplet manipulation for plug-and-play assembly, Adv. Funct. Mater. n/a (2024) 2416457, https://doi.org/10.1002/adfm.202416457.
[39] J.S. Bjørge, S.A. Bjørkheim, M.-M. Metallinou, T. Log, Ø. Frette, Influence of acetone and sodium chloride additives on cooling efficiency of water droplets impinging onto hot metal surfaces, Energies 12 (2019), https://doi.org/10.3390/en12122358.
[40] Z. Zhou, F. Yan, Z. Gengxin, D. Wu, H. Xu, A study on the dynamic collision behaviors of a hydrous ethanol droplet on a heated surface, Processes 11 (2023) 1804, https://doi.org/10.3390/pr11061804.
[41] X. Li, Z. Wang, D. Wei, Scavenging energy and information through dynamically regulating the electrical double layer, Adv. Funct. Mater. 34 (2024), https://doi.org/10.1002/adfm.202405520.